




Enhanced field-induced-strain by maximizing reversible domain switching contribution via eliminating negative strain in $(\text{Na}_{0.5}\text{Bi}_{0.5})\text{TiO}_3$ -based ceramics

Tianxiao Meng^{1,2}, Qingning Li^{2,*} , Changrong Zhou^{1,2,*}, Wei Li^{1,2}, Shuai Cheng^{1,2}, Changlai Yuan^{1,2}, Jiwen Xu^{1,2}, and Guanghui Rao^{1,2,*}

¹Guangxi Key Laboratory of Information Materials, Guilin University of Electronic Technology, Guilin 541004, Guangxi, People's Republic of China

²School of Material Science and Engineering, Guilin University of Electronic Technology, Guilin 541004, Guangxi, People's Republic of China

Received: 19 December 2021

Accepted: 26 January 2022

Published online:
12 February 2022

© The Author(s), under exclusive licence to Springer Science+Business Media, LLC, part of Springer Nature 2022

ABSTRACT

Ferroelectrics with high field-induced strain play a key role in the application of piezoelectric actuators. However, the strain contribution mainly originated from domain switching for normal ferroelectrics. As a result, the negative/remnant strain from irreversible domains orientation lowers the output strain, thus severely limiting their practical applications. Here, we optimized the output strain by maximizing reversible domain switching contribution via eliminating negative strain by composition design strategy. The maximum strain $S = 0.41\%$ with large signal piezoelectric coefficient $d_{33}^* = 688 \text{ pm/V}$ was achieved for $(\text{Bi}_{0.5}\text{Na}_{0.5})_{0.94}\text{Ba}_{0.06}\text{Ti}_{1-x}(\text{Nb}_{0.5}\text{Cr}_{0.5})_x\text{O}_3$ ceramics with $x = 0.035$. The enhanced total strain level was due to the critical composition where the dominating ergodic state was just established. Highly boosting domain switching during reversible phase transition from an ergodic relaxor to ferroelectric order at this critical composition led to the significant enhancement in the maximum usable strains. This study provides a novel and efficient guideline for developing environmentally friendly ceramics with high strain response.

Address correspondence to E-mail: liqnmk@guet.edu.cn; zcr750320@guet.edu.cn; rgh@guet.edu.cn

1 Introduction

Ferroelectric ceramics with the capability of generating large strain in response to an applied electric field were widely used as functional materials in high precision positioning devices [1–4]. Until now, lead-based piezoceramics were the widest applications materials in high-precision displacement actuators because of their high achievable electro-strains. Current driving to develop lead-free alternatives presents an urgent requirement to reduce the large harmful contents of toxic Pb in lead-based materials [3, 5–7]. $(\text{Bi}_{0.5}\text{Na}_{0.5})\text{TiO}_3$ (BNT)-based ceramics were regarded as a potential lead-free candidate for high-precision actuators because of high electro-strain performances [8–12].

As was well known, the electric-field-induced strain was a comprehensive result of intrinsic and extrinsic components [13]. The intrinsic contributions included lattice strain and piezoelectric effects, while extrinsic contributions related to the domain switching/domain wall movement [14]. The extrinsic component was usually regarded to be the dominating origin of excellent piezoelectric responses in BNT-based ceramics [15–18]. Thus instead, modulation ferroelectric domain and its piezoresponse was an important pathway to improve the piezoelectric response [3]. BNT-based ferroelectric ceramics generally exhibited butterfly strain-electric field (S - E) curves with large remnant or negative strains (S_N) due to the irreversible extrinsic contributions (domain switching), thus causing relatively low strains output [19].

Over the last several decades, strategies to enhance strain by constructing phase boundary (phase transition) [20–23] and heterogeneous microstructures [24] had been attempted to enhance large signal electromechanical properties in BNT-based piezoelectrics.

Lee et al. discovered that the total and negative strain increases with increasing ratio of BNT in $95\text{Bi}_{0.5}(\text{Na}_{0.75}\text{K}_{0.25})\text{TiO}_3$ - 5BiAlO_3 [25]. Dinh et al. reported that $(\text{Bi}_{0.47}\text{Na}_{0.47}\text{Ba}_{0.06})_{1-x}\text{La}_x\text{TiO}_3$ ($x = 0.02$) ceramics had a large total strain (S_{total}) of 0.457% [26]. However, the exceptionally peak-to-peak strains reported in butterfly strain-electric field (S - E) curves for BNT piezoceramics could not represent the available output strain, which was often considered as a shortcoming in actuator applications [27, 28]. Very recently, the results reported by Wei et al.,

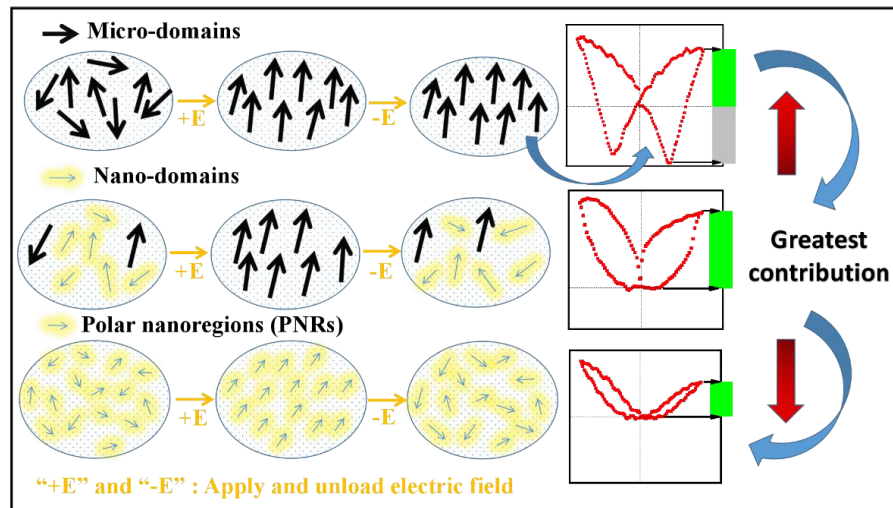
demonstrated that the large strain response was related to both the ergodic feature and suitable PNRs size [29]. Shi et al. showed that the resulting large strain was believed to be the result of the reversible relaxor to ferroelectric phase transition as well as the reorientation of the ferroelectric domains [30].

Although these strategies induced outstanding strain properties, the giant strain mechanism had been a long-standing debate. Specifically, the aforementioned reports neglected S_N contribution to the piezoelectric activity, indicating an indistinct understanding of the mechanism of extrinsic contributions. The S_N contribution was stem from the irreversible domain switching during the process of electric field unloading, which was tightly linked to remnant polarization and strain in the virgin ceramics caused by the first electric field cycle.

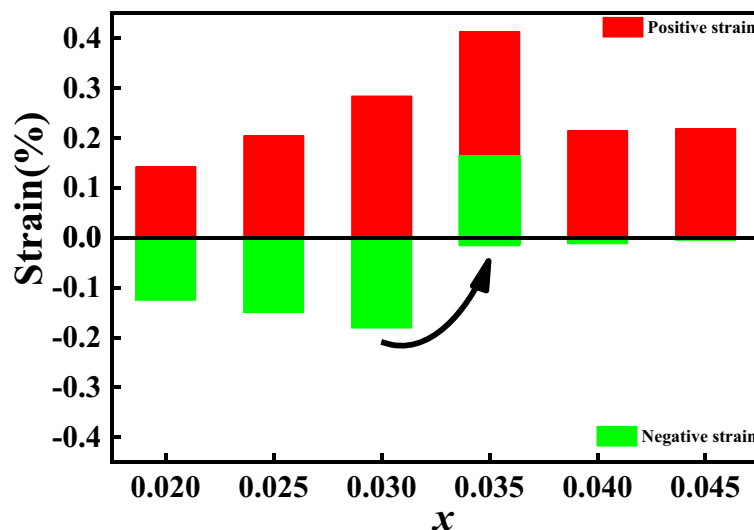
Based on the above discussion, a composition design strategy by introducing complex ions ($\text{Nb}_{0.5}\text{Cr}_{0.5}$)⁴⁺ into the morphotropic phase boundary (MPB) composition $(\text{Bi}_{0.5}\text{Na}_{0.5})_{0.94}\text{Ba}_{0.06}\text{TiO}_3$ (BNT-BT6) was adopted to obtain a critical state (predominant ergodicity) in which the field-induced ergodic relaxor to ferroelectric order transition was just established and disrupted respectively during electrical loading and unloading. At this critical point, the reoriented ferroelectric domains switched back completely at zero electric field with maximum domain switching contribution, thus giving rise to a significant enhancement of electro-strains with negligible negative strain. The design strategy of this work is shown in Fig. 1a, b. Therefore, the method of reducing negative strain to increase output strain in this study was beneficial to the development of lead-free ceramics with excellent electromechanical performance.

2 Experimental procedure

The conventional solid-state sintering process was used to make $(\text{Bi}_{0.5}\text{Na}_{0.5})_{0.94}\text{Ba}_{0.06}\text{Ti}_{1-x}(\text{Nb}_{0.5}\text{Cr}_{0.5})_x\text{O}_3$ (BNT-BT6- x NC, $x = 0, 0.01, 0.015, 0.02, 0.025, 0.03, 0.035, 0.04, 0.045, 0.05$) ceramics. The raw materials were Bi_2O_3 (99%), Na_2CO_3 (99.99%), BaCO_3 (99%), TiO_2 (99%), Nb_2O_5 (99.9%), Cr_2O_3 (99%). An appropriate amount of anhydrous ethanol was introduced to a ball mill tank containing zirconia balls with the required ratio for ball grinding for 24 h, according to stoichiometric weighing. After drying, the slurries were calcined at 840 °C for 2 h in the air. Then the



(a)



(b)

Fig. 1 **a** Schematic diagram showing the design principle of this work. **b** Working diagram of increasing positive strain by decreasing negative strain. ($x = 0.02, 0.025, 0.03, 0.035, 0.04, 0.045$)

calcined powders were granulated with 8 wt% of polyvinyl alcohol (PVA) as binders. The calcined powder was pressed into disks of 10 mm diameter and 0.5 mm thickness under 10 MPa. The green pellets were debonded at 600 °C for 2 h and sintered in the air at 1140 °C for 2.5 h. For the electrical properties test, Ag paint was applied to both faces of the ceramics and then fired at 600 °C for 30 min.

X-ray diffractometry (XRD, Bruker, D8-2-advance) with the Cu K α radiation was used to detect the phase structures of (Nb_{0.5}Cr_{0.5})⁴⁺ doped BNT-BT6 ceramics at room temperature. SEM (FEG-450, FEI,

USA) was used to examine the microstructure of the ceramics, and Nano Measurer software was used to measure the average grain size. The Raman spectrum was measured using a Lab RAM HR Evolution (Horiba JY, France). The temperature dependence of dielectric permittivity and loss was tested from 30 to 500 °C, using an LCR analyzer (Keysight, 4980 A). The poling process of ceramics was performed under a DC field of 40 kV/cm at room temperature for 10 min in a silicone oil bath, and the piezoelectric constant (d_{33}) was tested via a quasistatic piezo- d_{33} meter (ZJ-3A, CAS, Shanghai, China) after 24 h. The

electric-field-induced polarization and strain measurements were carried out at 1 Hz using a ferroelectric test unit (TFANAYLZER 2000HS, aixACCT Systems GmbH, Aachen, Germany).

3 Results and discussion

Figure 2a displayed the XRD patterns of BNT-BT6- x NC ceramics at room temperature. All samples exhibited a typical perovskite structure without any secondary impurity phases, suggesting that NC dissolved into the BNT-BT6 lattice. Figure 2b shows the magnified diffraction peaks of 38°–48°. For the sample $x = 0$, both (111) and (200) diffraction peaks split into double peaks, verifying their polymorph structure of rhombohedral R3c and tetragonal P4bm symmetries. The coexistence of rhombohedral and tetragonal phase for BNT-BT ceramic was in accordance with literature reports on MPB of BNT-BT ceramics [31–36]. However, the split peaks evolved towards the single peak with an asymmetry in the left side with increasing doping content, indicating the transition from coexistence phases to cubic-like phase with rhombohedral/tetragonal distortion [29].

Figure 3 depicted the room temperature Raman spectra of BNT-BT6- x NC ceramics, which further confirmed the phase transition behavior of the examined materials. The Raman spectra revealed four major regions: (1) The mode below 200 cm^{-1} was connected to A-site vibrations such as Bi^{3+} , Na^{+} .

(2) The peak at 260 cm^{-1} was associated with the Ti–O bond. (3) The 450 to 700 cm^{-1} modes were ascribed to TiO_6 octahedra vibrations. (4) The frequency range above 700 cm^{-1} was associated with the superposition of alternating vibration A_1 (longitudinal optical) and E (longitudinal optical) bands [37–39]. Furthermore, two bands around 260 and 325 cm^{-1} gradually broadened with increasing x , which might associate with the tetragonal to cubic-like phase transition as well as the formation of polar nanoregions (PNRs) [29]. The decrease in the number of vibrational modes revealed the structural symmetry of the ceramics was enhanced as x increased [40, 41], which was consistent with the XRD results.

The morphology of BNT-BT6- x NC ceramics is displayed in Fig. 4a–j, all the obtained ceramics were well sintered. Figure 4k shows that the average grain size of BNT-BT6- x NC increased from 2.79 μm up to 8.43 μm with increased NC content from 0 to 25 mol% initially, and then decreased to 2.80 μm . This result indicated that low NC content could promote grain growth. Excessive addition could restrain the grain growth. The large grain size could be beneficial for domain switching and excellent piezoelectric properties [42, 43].

Figures 5 and S1 presented the dielectric permittivity (ϵ_r) of unpoled and poled BNT-BT6- x NC ceramics as a function of temperature from 30 to 200 °C collected at different frequencies of 500, 1 k, 10 k, 50 k, 100 k, and 200 k Hz (Fig. S1 of Supplemental Material). For all unpoled specimens, a

Fig. 2 Room temperature X-ray diffraction patterns of BNT-BT6- x NC ceramics with 2θ ranging over a 20°–80°, b 38°–48°

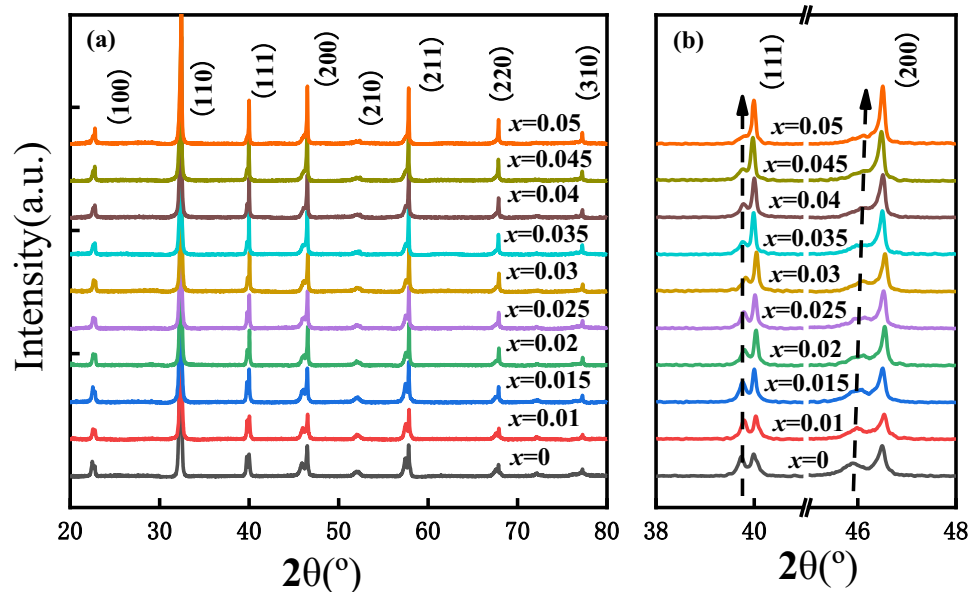
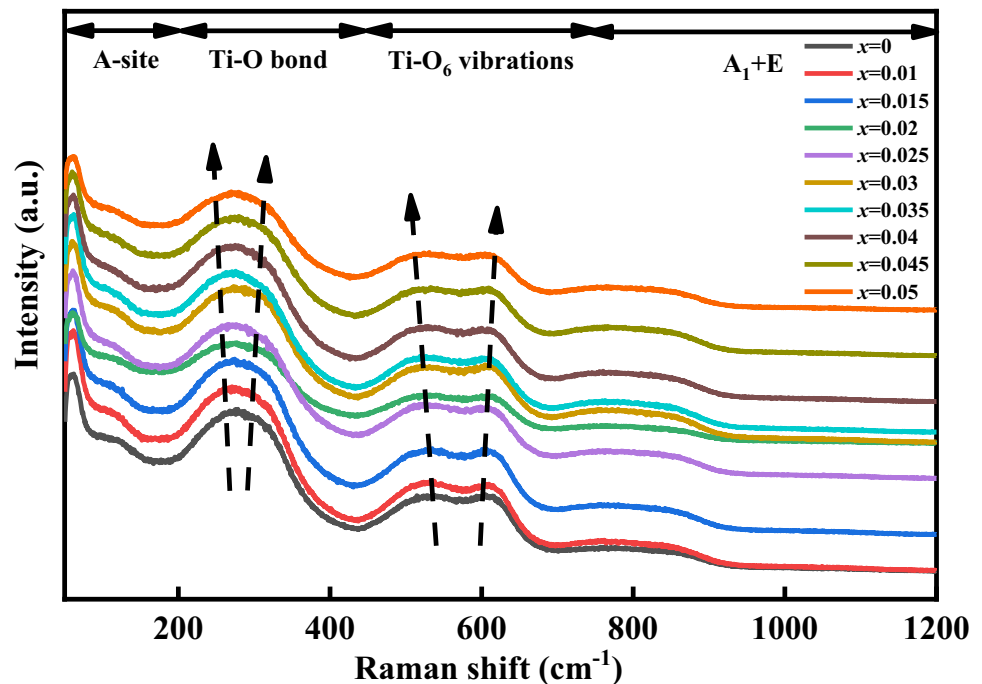


Fig. 3 Room temperature Raman spectra of BNT-BT6- x NC ceramics



considerable frequency-dependent dispersion from 30 up to 200 °C was observed, classifying the ceramics as relaxor ferroelectrics. However, a dielectric anomalous peak T_{F-R} for poled $x < 0.035$ samples with a very weak frequency-dependent dispersion and decreased dielectric permittivity occurred in the low temperature area. The anomalous peak at T_{F-R} represented the transition temperature between the ferroelectric and relaxor phases [44]. It was suggested that BNT-BT6- x NC ceramics with $x < 0.035$ were non-ergodic relaxor ferroelectrics state undergoing a field-induced phase transition to a long-range ordered state, which produced a huge negative strain. This meant that the initially nanoscale domains regions grew into micron-sized domains accompanied by irreversible transitions with the application of an electric field [45]. It was also worth noting that the frequency-dependent dispersion and dielectric permittivity for unpoled and poled specimens of $x > 0.035$ showed subtle changes. These results implied a transition from an irreversible state ($x < 0.035$) to a reversible state ($x > 0.035$) by comparison before and after poled samples.

Figure 6a depicted the bipolar strain curves (S - E) of BNT-BT6- x NC ceramics at 1 Hz. The samples with $x = 0$ –0.03 showed butterfly shaped strain (S)- field (E) loops with a relatively large negative strain, demonstrating its non-ergodic nature [29]. With the

complex cations NC substitution increasing, the S - E loops changed into sprout-shaped ones ($x \geq 0.035$), demonstrating the transition from non-ergodic to ergodic states. The effects of NC content on the positive strain (S_{pos}) and negative strain (S_{neg}) are contrasted in Fig. 6b. It could be noticed that the S_{pos} and S_{neg} changed slightly at content $x < 0.025$; when $0.025 < x < 0.035$, the S_{pos} and S_{neg} increased. At $x = 0.035$, the S_{neg} vanished and a large field-induced strain S_{pos} of 0.41% was obtained. The decrease of the S_{neg} implied the reduction of the irreversible domain switching and the weakening of the interaction between polar nanoregions (PNRs). As the doping content continued to increase ($x > 0.035$), the contribution of the S_{pos} began to decrease, which was ascribed to the ordered arrangement of weakly correlated PNRs. These results were compared to previous research on the strain and normalized strain (S_{max}/E_{max}) of lead-free functional ceramics, as indicated in Table 1 [29, 46–56]. The strain value of 0.41% in this work located at a relatively high level among these lead-free ceramics.

Figure 6c further depicted in detail the evolution of reversible domain switching at various strain response stages when an electric field was applied at $x = 0.035$. From point a to point b, a virgin state characterized by a random polydomain pattern with micro-domains and nano-domains was displayed.

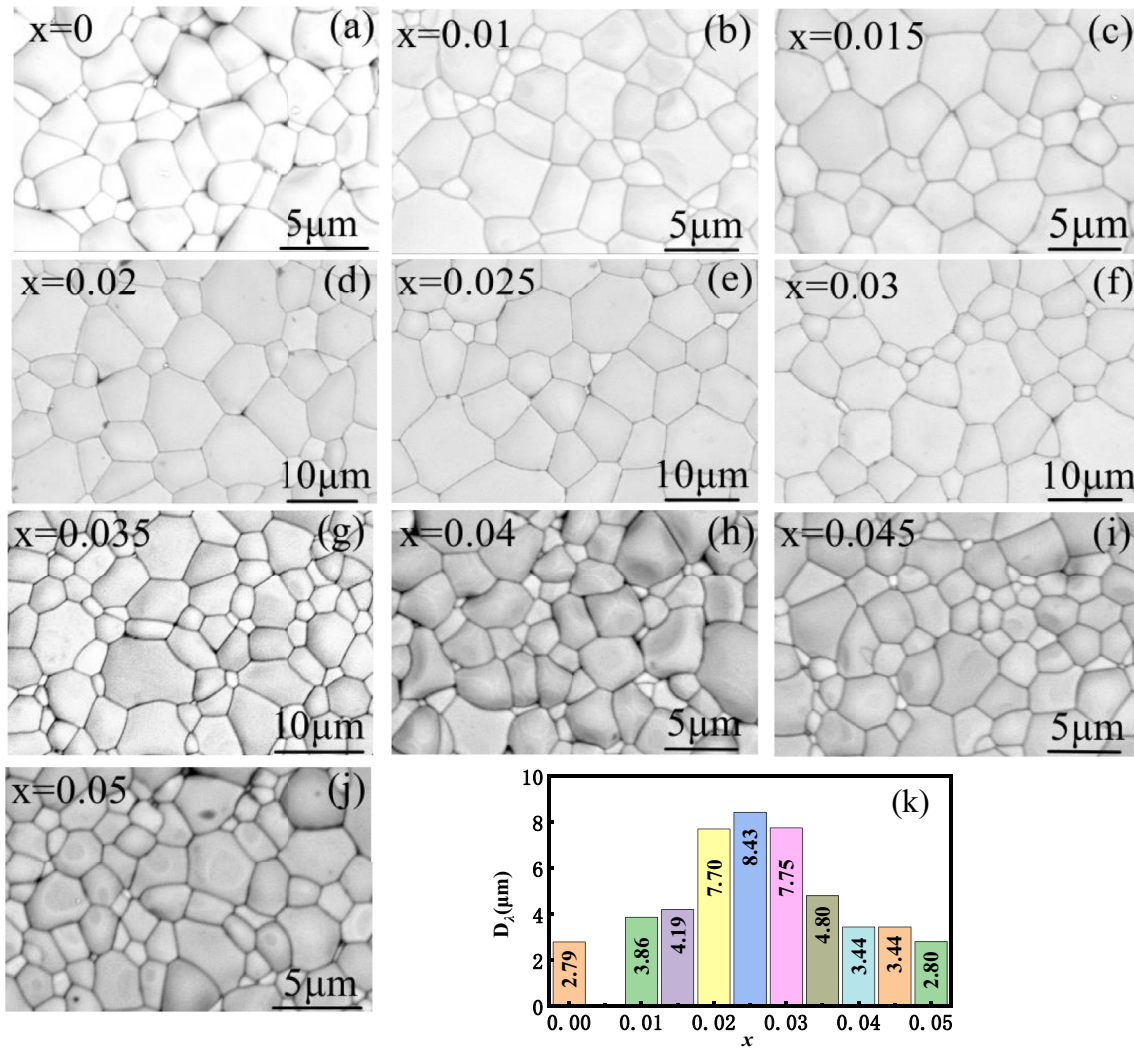


Fig. 4 SEM images of the as-sintered BNT-BT6- x NC ceramics with **a** $x = 0$, **b** $x = 0.01$, **c** $x = 0.015$, **d** $x = 0.02$, **e** $x = 0.025$, **f** $x = 0.03$, **g** $x = 0.035$, **h** $x = 0.04$, **i** $x = 0.045$, **j** $x = 0.05$ and **(k)** diagram of average grain size

However, the electric field strength was not high enough to promote appreciable domains motion. It was shown that the macroscopic properties of this stage were caused by a slight displacement of ions (or complexes) in the crystal lattice [13]. Further increase of the electric field resulted in an increase in the nonlinearity of the strain curves due to the directional arrangement and growth of reversible and irreversible domains. Once domain switching saturated at point c, further increase in applied electric field activated only an intrinsic response which led to a linear increase in strain. Once the electric field was removed, domains will mostly be switched back to the crystallographically allowed orientations at point d. When the electric field was unloaded to zero (point e), the dynamic stability of the domain was

influenced by the driving restoring force provided by the weakly correlated PNRs, which led to the emergence of critical ferroelectric states dominated by ergodic states in the zero field. However, there were always a small number of domains that cannot be restored to the initial state, so that point e cannot coincide with point a. In general, domain switching greatly promoted the continuous hysteresis phenomenon, and the disappearance of negative strain showed the reversibility of domain switching.

Figure 7a presented the composition dependent I - E loops of BNT-BT6- x NC ceramics with the application of an alternating electric field of 60 kV/cm. In the I - E loops, two current peaks emerged during the application of the electric field (named as “ P_1 ”, “ P_2 ”). The current peak (P_1) could be ascribed to the

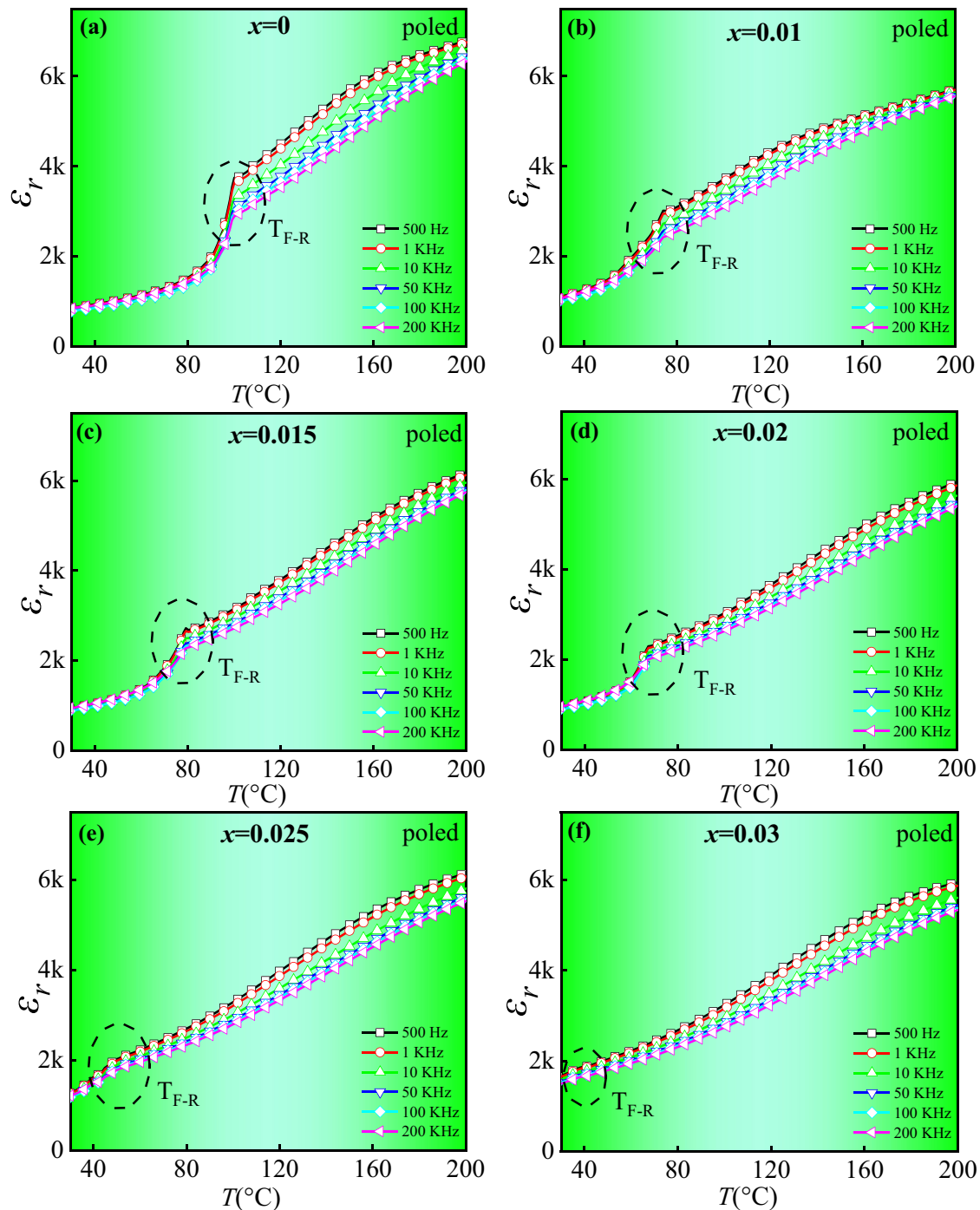


Fig. 5 Temperature dependence of dielectric constant for the poled BNT-BT6- x NC ceramics

ferroelectric domains switching [57]. The current peaks at P_2 implied the existence of weakly polar tetragonal phase [58]. The appearance of two current peaks could be attributed to the coexistence of non-ergodic and ergodic phases [59, 60]. With the increase

of the NC content, a critical state that the P_1 peak shifting to zero field was established at $x = 0.035$. At the boundary of ergodic and non-ergodic phases ($x = 0.035$), the strain value reached the maximum with the disappearance of negative strain, indicating

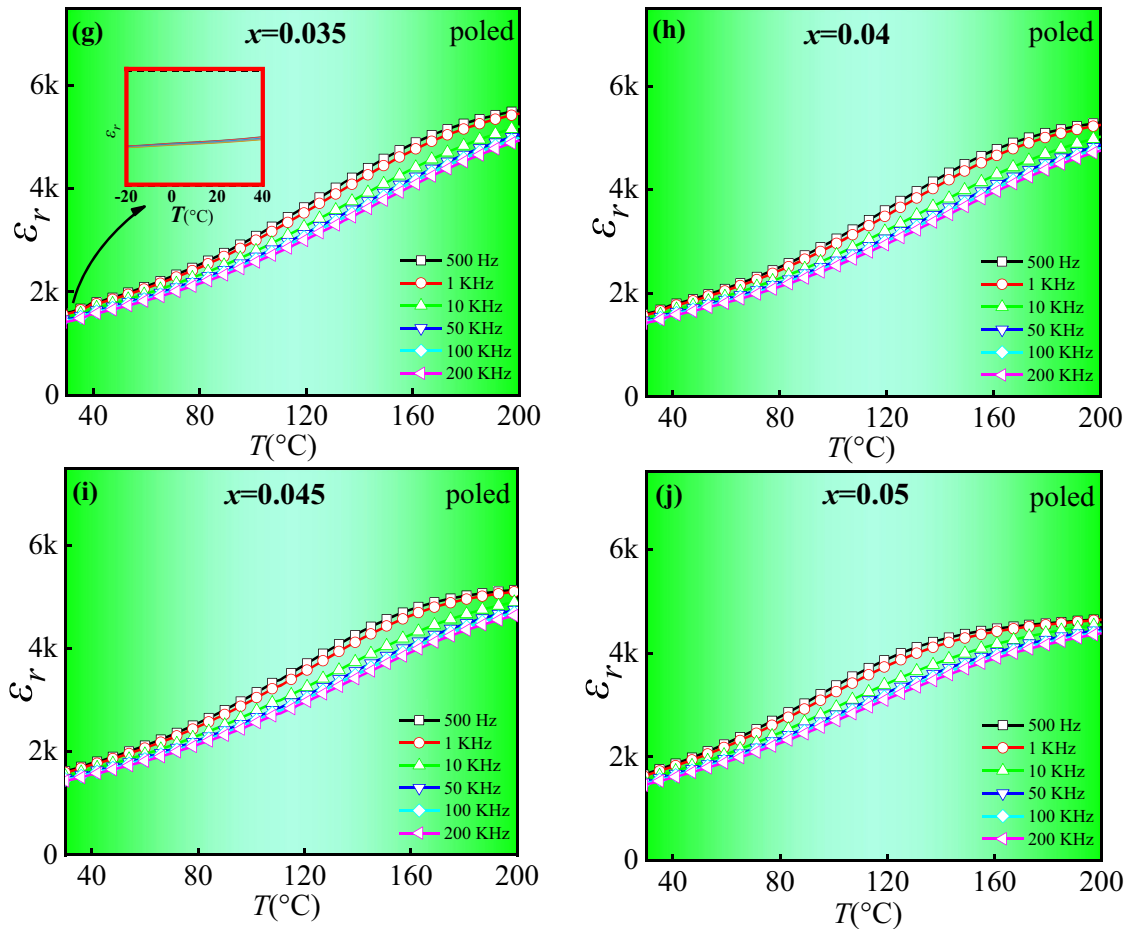


Fig. 5 continued

that the ergodic state was dominant (Fig. 7b). In addition, the domains could more easily switch back to an initial state when the applied electric field was removed.

The remnant polarization and strain generated in the first cycle at 60 kV/cm are shown in Fig. 8. When $x < 0.035$, the weak compositional dependence of the remnant polarization and strain suggested that the irreversible domain switching was dominant in the non-ergodic state. At the critical component point $x = 0.035$, the remnant polarization dropped suddenly, suggesting a phase transition from a non-ergodic to an ergodic state. Meanwhile, the remnant strain decreased to zero, which could be attributed to the driving force of the dominant ergodic state.

Rayleigh analysis was utilized to further study the reversible domain switching contribution produced by complex cations $(\text{Nb}_{0.5}\text{Cr}_{0.5})^{4+}$ doping. The piezoelectric effect was defined as the linear

relationship between applied stress and resulting dielectric displacement, or applied electric field and resulting mechanical strain. Rayleigh analysis was a popular method for determining the contribution of domain wall motion to the dielectric or piezoelectric response of piezoelectric ceramics [61]. Figure 9a shows composition variation of the dielectric coefficients in the sub-coercive field. The magnitude of the property (dielectric or piezoelectric) in the sub-coercive field region was proportional to the amplitude of the field. As a result, the dielectric coefficient was determined by the relationship:

$$\epsilon_r = \epsilon_{rev} + \alpha_\epsilon (E_{max} - E_{min}) \tag{1}$$

Generally, the dielectric coefficient was calculated using the expression:

$$\epsilon_r = \frac{P_{max} - P_{min}}{E_{max} - E_{min}} \tag{2}$$

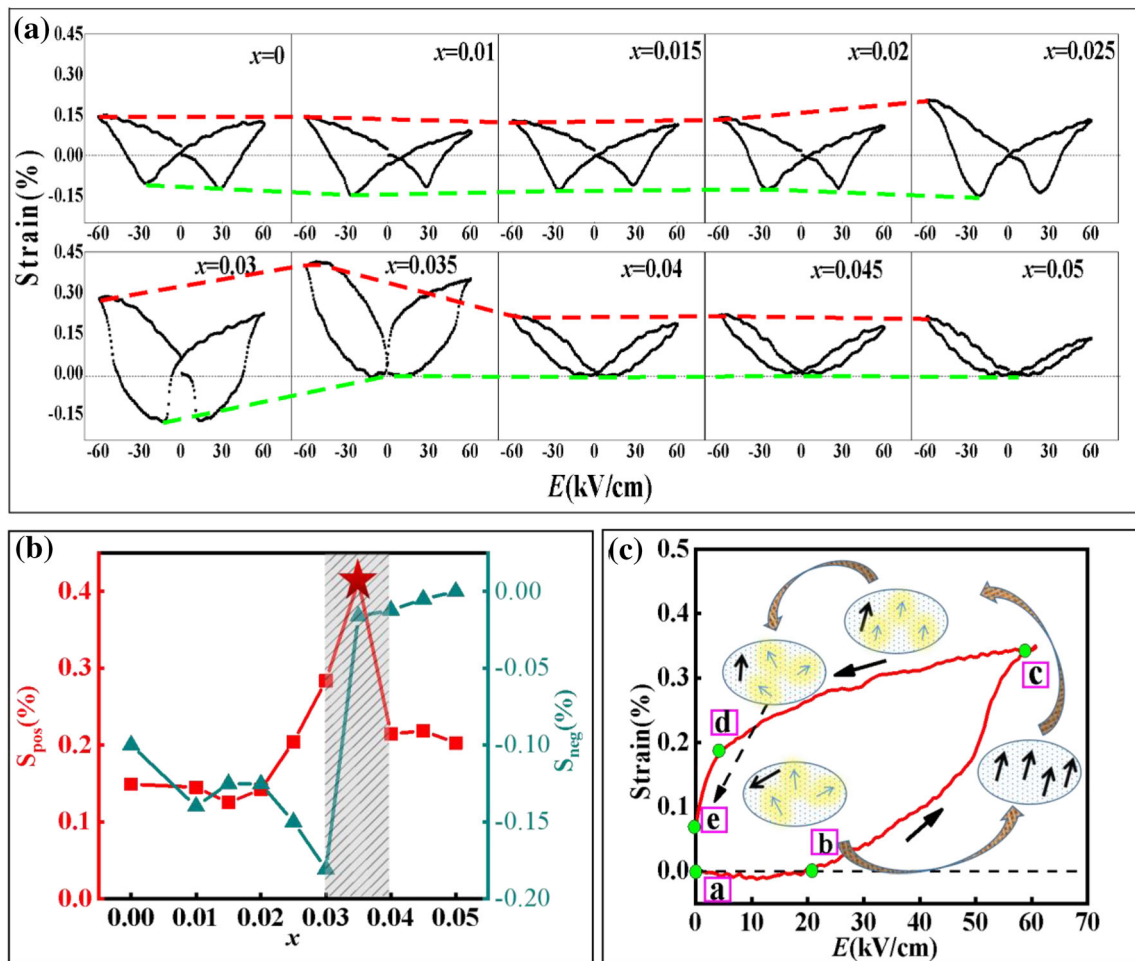


Fig. 6 **a** Composition dependence of bipolar field-induced strain; **b** The change law of positive strain and negative strain with different components; **c** The applied electric field's reversible domain switching history at $x = 0.035$

Table 1 This research is compared to previous reports on the strain characteristics of ceramics

Composition	Strain (%)	E (kV/cm)	d_{33}^* (pm/V)	References
BF-BT-Fe	0.34	50	510	[46]
BF-BT-Sb	0.168	50	336	[47]
BNKT-BT	0.37	60	630	[48]
BNT-ST-Mn	0.22	60	367	[49]
NBT-KT-BT	0.30	50	600	[50]
BNKLSTT-La	0.322	80	403	[51]
NBST-FN	0.26	70	371	[52]
BNT-BT-KNN-CuO	0.39	50	780	[53]
BNT-BT-NZ	0.65	80	813	[29]
BNT-BT-AS	0.46	80	573	[54]
BNT-BKHT	0.41	60	683	[55]
BNBT-Er-FS	0.465	65	713	[56]
BNT-BT-NC	0.41	60	688	This work

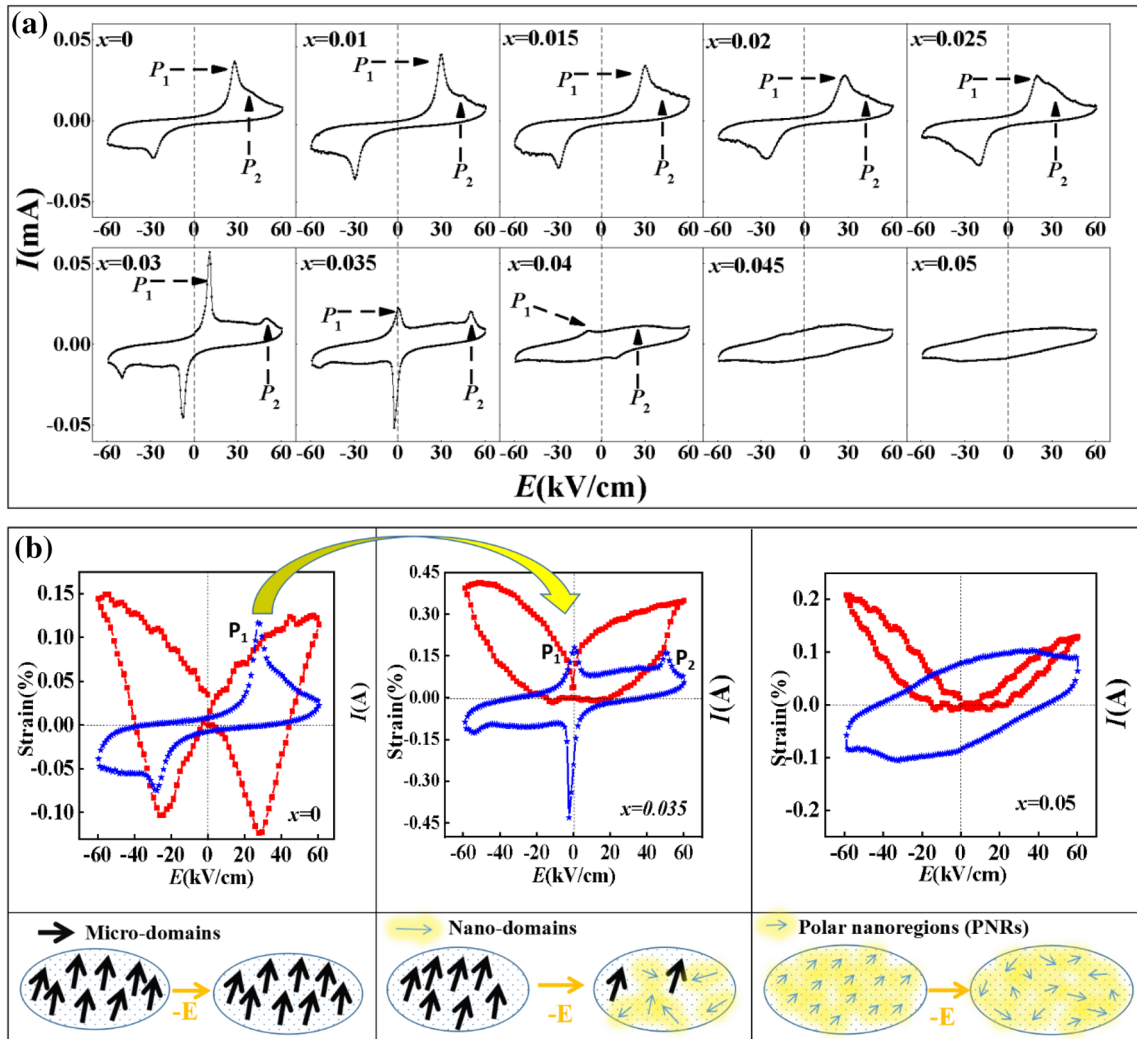


Fig. 7 **a** Composition dependence of *I*-*E* loops; **b** Schematic diagram of component engineering regulation results

where α_e was the dielectric Rayleigh coefficient, ϵ_{rev} was the initial dielectric permittivity which was a field-independent term, and ϵ_r was the measured relative dielectric permittivity. $P_{max} - P_{min}$ corresponded to the inter-peak polarization of $E_{max} - E_{min}$. The reversible coefficient ϵ_{rev} stabilized in the $0.01 < x < 0.05$ range between 1400 and 1900. The irreversible coefficient α_e exhibited a general negative trend, as illustrated in Fig. 9b. We can define a term f_{irrev} as the fraction of the irreversible contribution to the measured dielectric response:

$$f_{irrev} = \frac{\epsilon_{irreversible}}{\epsilon_{reversible} + \epsilon_{irreversible}} = \frac{\alpha_e E_{max}}{\epsilon_{rev} + \alpha_e E_{max}} \quad (3)$$

This allowed us to calculate the proportion of the irreversible contribution of various composition points (as shown in Fig. 9c). The portion of

irreversible contribution dropped from 58.54 to 36.77% when the concentration of $(\text{Nb}_{0.5}\text{Cr}_{0.5})^{4+}$ complex cations increased. It was therefore concluded that the rapid decline of α_e and f_{irrev} was due to a lower contribution of irreversible domain wall displacements. In conclusion, the $(\text{Nb}_{0.5}\text{Cr}_{0.5})^{4+}$ doping in BNT-BT6 had successfully reduced the effect of external contribution and optimized the reversible domain switching contribution.

Figure 10 displayed the piezoelectric constant (d_{33}), positive maximum strain (S_{max}), and large signal strain d_{33}^* (S_{max}/E_{max}) for BNT-BT6-*x*NC ceramics. The piezoelectric constant d_{33} first increased and then sharply decreased with increasing *x*, and reached maximum values of 181 pC/N at $x = 0.025$. The destabilization of ferroelectric long-range order upon approaching the critical content of $x = 0.03$ was

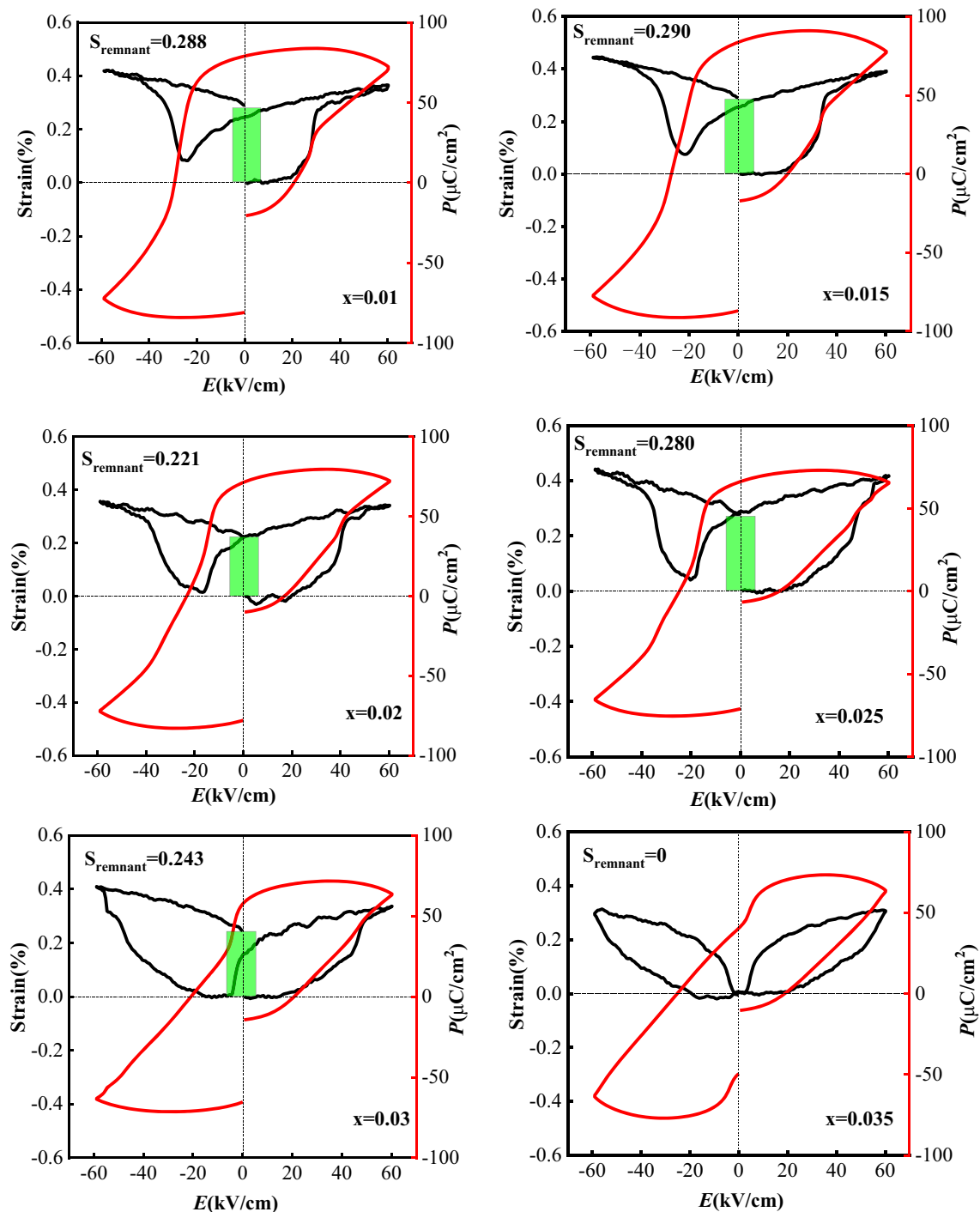


Fig. 8 Shows the variation of different remnant strain and polarization with respect to composition. ($x = 0.01, 0.015, 0.02, 0.025, 0.03, 0.035$)

visible in the weak field piezoelectric response. In addition, it could be observed that the $x = 0 \sim 0.03$ ceramics exhibited saturated butterfly shaped bipolar strain curve at room temperature, which transformed to the sprout-shaped curves with negligible S_{neg} for

$x = 0.035$ ceramics. Especially, the d_{33} decreased sharply and d_{33}^* increased rapidly for $x > 0.03$. Based on the above results, it could be seen that the large strain was just located at the ergodic and nonergodic phase boundary, and it was accompanied by the

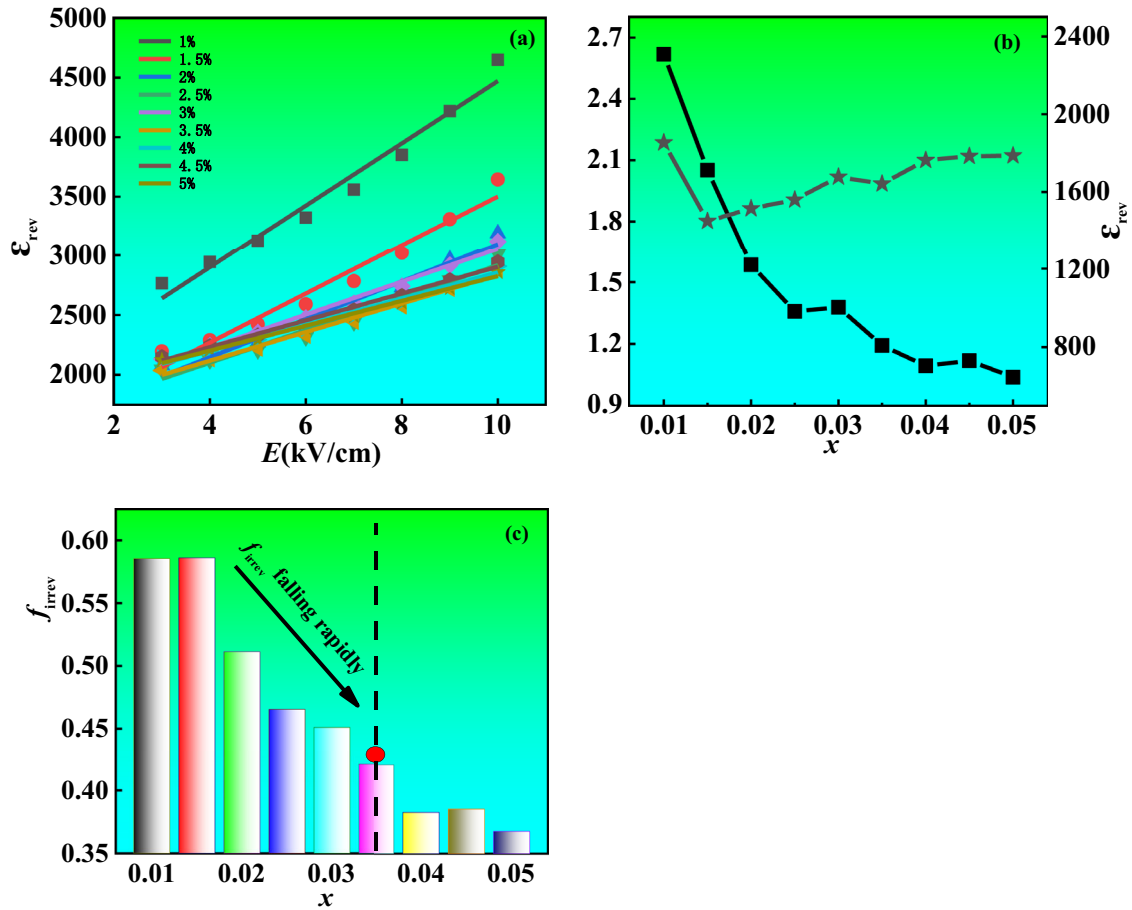


Fig. 9 a Shows the corresponding fitted results of Rayleigh parameters at room temperature with a series of electric field strength from 3 to 10 kV/cm. b the irreversible coefficient α_e and

reversible coefficient ϵ_{rev} with respect to composition. c The portion of irreversible contribution

critical transition from nonergodic state to dominate ergodic state [35]. Interestingly, the largest d_{33} values mainly originated from the irreversible polarization left after poling. However, the largest d_{33}^* required the recoverability of domain switching. Therefore, it was suggested that a critical non-ergodic to ergodic transition was obtained by the doping of NC complexes. When ergodic states dominated, the contribution of reversible domain switching was maximized and a large strain response was acquired.

4 Conclusions

In this work, the electro-strain properties of lead-free BNT-BT6- x NC ceramic system ($0.01 \leq x \leq 0.05$) were systematically investigated. A large field-induced strain of 0.41% as well as d_{33}^* of 688 pm/V under an electric field of 60 kV/cm was obtained with

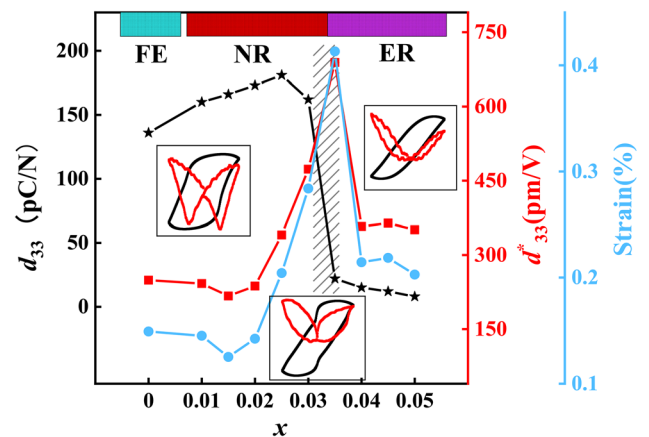


Fig. 10 Piezoelectric coefficient (d_{33}), positive maximum strain and large signal strain (d_{33}^*) for the BNT-BT6- x NC ceramics

$x = 0.035$. The experiments and analysis showed that the domain switching activity was greatly enhanced during the reversible phase transition from an

ergodic relaxor to ferroelectric order at $x = 0.035$, which was beneficial for the promotion of the usable output strains. The enhanced electro-strain performance was tightly associated with the dominating ergodic state as well as minimized negative strain which was induced by the critical $(\text{Nb}_{0.5}\text{Cr}_{0.5})^{4+}$ doping content. As a result, the output strain of the BNT-BT6- x NC ceramics was enhanced through achieving maximum contribution of reversible domain switching and eliminating negative strain by chemical modification strategy. The strategy provided an effective way to enhance the large strain response of the eco-friendly high-precision actuators.

Acknowledgements

This work was supported by the National Nature Science Foundation of China (51862004) and the Natural Science Foundation of Guangxi (2017GXNSFDA198024) and Foundation for Guangxi Bagui scholars.

Author contributions

All authors contributed to the study conception and design. Material preparation, data collection and analysis were performed by TM, QL, CZ, WL, SC, CY, JX, GR. The first draft of the manuscript was written by TM, CZ, QL and all authors commented on previous versions of the manuscript. All authors read and approved the final manuscript.

Data availability

The data that support the findings of this study are available from School of Materials, Guilin University of Electronic Science and Technology, but restrictions apply to the availability of these data, which were used under license for the current study, and so are not publicly available. Data are however available from the authors upon reasonable request and with permission of Pro. Dr. Qingning Li.

Declarations

Conflict of interest No conflict of interest exists in the submission of this manuscript, and this manuscript is approved by all authors for publication. I

would like to declare on behalf of my coauthors that the work described was original research that has not been published previously, and not under consideration for publication elsewhere, in whole or in part. All the authors listed have approved the manuscript that is enclosed. The authors declare that they have no known competing financial interests or personal relationships that could have appeared to influence the work reported in this paper.

Supplementary Information: The online version contains supplementary material available at <http://doi.org/10.1007/s10854-022-07857-y>.

References

1. D. Shi, Q. Zhang, Y. Ye, L. Luo, E.K. Cheng, D. Lin, K.-H. Lam, *Measurement* **104**, 287–293 (2017)
2. K. Wang, F.-Z. Yao, W. Jo, D. Gobeljic, V.V. Shvartsman, D.C. Lupascu, J.-F. Li, J. Rödel, *Adv. Funct. Mater.* **23**, 4079–4086 (2013)
3. J. Hao, W. Li, J. Zhai, H. Chen, *Mater. Sci. Eng. R Rep.* **135**, 1–57 (2019)
4. H. Qi, A. Xie, J. Fu, R. Zuo, *Acta Mater.* **208**, 116710 (2021)
5. J. Rödel, W. Jo, K.T.P. Seifert, E.-M. Anton, T. Granzow, D. Damjanovic, *J. Am. Ceram. Soc.* **92**, 1153–1177 (2009)
6. W. Jo, S. Schaab, E. Sapper, L.A. Schmitt, H.-J. Kleebe, *J. Appl. Phys.* **110**, 074106 (2011)
7. W. Bai, P. Zheng, F. Wen, J. Zhang, D. Chen, J. Zhai, Z. Ji, *Dalton Trans.* **46**, 15340–15353 (2017)
8. W. Cao, W. Li, Y. Feng, T. Bai, Y. Qiao, Y. Hou, T. Zhang, Y. Yu, W. Fei, *Appl. Phys. Lett.* **108**, 202902 (2016)
9. T. Li, X. Lou, X. Ke, S. Cheng, S. Mi, X. Wang, J. Shi, X. Liu, G. Dong, H. Fan, Y. Wang, X. Tan, *Acta Mater.* **128**, 337–344 (2017)
10. W. Bai, D. Chen, P. Zheng, J. Zhang, B. Shen, J. Zhai, Z. Ji, *Ceram. Int.* **43**, 3339–3345 (2017)
11. W. Jo, J.E. Daniels, J.L. Jones, X. Tan, P.A. Thomas, D. Damjanovic, J. Rödel, *J. Appl. Phys.* **109**, 014110 (2011)
12. Z. Zhu, L. Luo, F. Wang, P. Du, X. Zhou, Q. Zhang, W. Li, Y. Wang, *J. Eur. Ceram. Soc.* **40**, 689–698 (2020)
13. G. Viola, T. Saunders, X. Wei, K.B. Chong, H. Luo, M.J. Reece, H. Yan, *J. Adv. Dielectr.* **03**, 1350007 (2013)
14. M. Abebe, K. Brajesh, R. Ranjan, *J. Appl. Phys.* **122**, 034101 (2017)
15. X. Liu, X. Tan, *Adv. Mater.* **28**, 574–578 (2016)
16. L. Zhang, H. Wang, D. Wang, M. Guo, X. Lou, D. Wang, *Adv. Funct. Mater.* **30**, 2004641 (2020)

17. T. Li, C. Liu, X. Ke, X. Liu, L. He, P. Shi, X. Ren, Y. Wang, X. Lou, *Acta Mater.* **182**, 39–46 (2020)
18. G. Li, G. Ge, J. Lin, C. Shi, F. Yan, K. Zhu, Y. Shi, B. Shen, J. Zhai, *Appl. Mater. Today.* **26**, 101332 (2022)
19. R. Dittmer, W. Jo, J. Rödel, S. Kalinin, N. Balke, *Adv. Funct. Mater.* **22**, 4208–4215 (2012)
20. J. Janbua, S. Niemchareon, R. Muanghlua, N. Vittayakorn, *Ferroelectrics* **490**, 13–22 (2016)
21. J.U. Rahman, A. Hussain, A. Maqbool, T.K. Song, W.J. Kim, S.S. Kim, M.H. Kim, *Curr. Appl. Phys.* **14**, 331–336 (2014)
22. W. Bai, D. Chen, Y. Huang, B. Shen, J. Zhai, Z. Ji, *J. Alloys Compd.* **667**, 6–17 (2016)
23. J. Hao, Z. Xu, R. Chu, W. Li, P. Fu, J. Du, G. Li, *J. Eur. Ceram. Soc.* **36**, 4003–4014 (2016)
24. C. Zhou, Y. Zhang, Y. Wang, Q. Li, J. Xu, G. Chen, C. Yuan, G. Rao, *J. Mater. Chem. C* **7**, 8255–8260 (2019)
25. D.S. Lee, S.J. Jeong, M.S. Kim, J.H. Koh, *J. Appl. Phys.* **112**, 124109 (2012)
26. T.H. Dinh, H.-S. Han, V.D.N. Tran, V.L. Van, N.B. Hung, J.-S. Lee, *J. Electron. Mater.* **49**, 6080–6086 (2020)
27. X. Geng, J. Zhang, R. Wang, X. Deng, L. Sun, Z. Gu, S. Zhang, *J Am Ceram Soc.* **100**, 5659–5667 (2017)
28. Y. Guo, H. Fan, C. Long, J. Shi, L. Yang, S. Lei, *J Alloys Compd.* **610**, 189–195 (2014)
29. Q. Wei, M. Zhu, M. Zheng, Y. Hou, *J. Alloys Compd.* **782**, 611–618 (2019)
30. J. Shi, H. Fan, X. Liu, Q. Li, *J. Eur. Ceram. Soc.* **34**, 3675–3683 (2014)
31. C. Wang, Q. Li, W. Zhang, H. Fan, *J. Mater. Sci. Technol.* **45**, 15–22 (2020)
32. H. He, W. Lu, J.A.S. Oh, Z. Li, X. Lu, K. Zeng, L. Lu, *ACS. Appl. Mater. Int.* **12**, 30548–30556 (2020)
33. X. Ren, H. Yin, Y. Tang, H. Fan, H. Yuan, *Ceram. Int.* **46**, 1876–1882 (2020)
34. M. Hinterstein, M. Hoelzel, J. Rouquette, J. Haines, J. Glaum, H. Kungle, M. Hoffman, *Acta Mater.* **94**, 319–327 (2015)
35. C. Zhou, Q. Li, J. Xu, L. Yang, W. Zeng, C. Yuan, G. Chen, *J. Am. Ceram. Soc.* **101**, 1554–1565 (2018)
36. M. Hinterstein, K.-Y. Lee, S. Esslinger, J. Glaum, A.J. Studer, M. Hoffman, M.J. Hoffmann, *Phys Rev B.* **99**, 174107 (2019)
37. Q. Li, C. Wang, W. Zhang, H. Fan, *J. Mater. Sci.* **54**, 4523–4531 (2018)
38. Q. Wei, M. Zhu, L. Li, Z. Guo, M. Zheng, Y. Hou, *J. Alloys Compd.* **731**, 631–635 (2018)
39. K. McLaughlin, C.P. Gonzalez, D. Wang, A. Feteira, *J. Alloys Compd.* **779**, 7–14 (2019)
40. J. Hao, W. Bai, W. Li, B. Shen, J. Zhai, *J. Appl. Phys.* **114**, 044103 (2013)
41. S. Jiao, F. Chen, Y. Zhang, Z. Hu, Z. Duan, F. Wang, D. Sun, *J. Am. Ceram. Soc.* **102**, 2791–2799 (2018)
42. J. Hao, W. Bai, W. Li, J. Zhai, *J. Am. Ceram. Soc.* **95**, 1998–2006 (2012)
43. Y. Tan, G. Viola, V. Koval, C. Yu, A. Mahajan, J. Zhang, H. Zhang, X. Zhou, N.V. Tarakina, H. Yan, *J. Eur. Ceram. Soc.* **39**, 2064–2075 (2019)
44. W. Bai, P. Li, L. Li, J. Zhang, B. Shen, J. Zhai, *J. Alloys Compd.* **649**, 772–781 (2015)
45. J. Xu, Q. Li, C. Zhou, W. Zeng, J. Xiao, J. Ma, C. Yuan, G. Chen, G. Rao, X. Li, *J. Electron. Mater.* **45**, 2967–2973 (2016)
46. F. Zeng, Y. Zhang, Z. Tu, X. Ge, F. Wang, M. Hao, J. Zhang, Y. Wang, X. Chen, W. Lu, G. Fan, *Ceram. Int.* **47**, 14097–14106 (2021)
47. F. Kang, L. Zhang, L. He, Q. Sun, Z. Wang, R. Kang, P. Mao, C. Zhu, J. Wang, *J. Alloys Compd.* **864**, 158917 (2021)
48. P. Jaita, P. Jarupoom, *J. Asian. Ceram. Soc.* **9**, 975–987 (2021)
49. W. Cao, W. Li, Q. Lin, D. Xu, *J. Mater. Sci. Mater. Electron.* **32**, 17645–17654 (2021)
50. W. Cao, J. Sheng, D. Xu, W. Li, *J. Mater. Sci. Mater. Electron.* **32**, 9500–9508 (2021)
51. A. Deng, J. Wu, *J. Eur. Ceram. Soc.* **41**, 5147–5154 (2021)
52. Y. Zhang, P. Fan, H. Li, J. Zhang, J. Xu, M. Li, X. Zhang, Z. Wei, J. Xu, L. Zhao, Y. Lu, H. Zhang, *Ceram. Int.* **47**, 17915–17920 (2021)
53. Z. Zhao, R. Ge, Y. Dai, *JAD.* **09**, 07 (2019)
54. L. Li, J. Hao, Z. Xu, W. Li, R. Chu, *Mater Lett.* **184**, 152–156 (2016)
55. C. Wang, X. Lou, T. Xia, S. Tian, *Ceram. Int.* **43**, 9253–9258 (2017)
56. J. Yang, Z. Xu, C. Zhu, H. Yu, D. Wang, X. Zhang, R. Chu, J. Hao, *J. Mater. Sci. Mater. Electron.* **31**, 21632–21639 (2020)
57. F. Li, R. Zuo, D. Zheng, L. Li, *J. Am. Ceram. Soc.* **98**, 811–818 (2015)
58. Q. Xu, T. Li, H. Hao, S. Zhang, Z. Wang, M. Cao, Z. Yao, H. Liu, *J. Eur. Ceram. Soc.* **35**, 545–553 (2015)
59. C. Wang, Q. Li, A.K. Yadav, H. Peng, H. Fan, *J. Alloys Compd.* **803**, 1082–1089 (2019)
60. G. Viola, H. Ning, X. Wei, M. Deluca, A. Adomkevicius, *J. Appl. Phys.* **114**, 1 (2013)
61. A. Pramanick, D. Damjanovic, J.E. Daniels, J.C. Nino, J.L. Jones, *J. Am. Ceram. Soc.* **94**, 293–309 (2011)

Publisher's Note Springer Nature remains neutral with regard to jurisdictional claims in published maps and institutional affiliations.